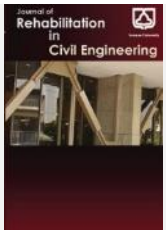

Journal of Rehabilitation in Civil Engineering

Journal homepage: https://civiljournal.semnan.ac.ir/

Optimum Robust Design of 2D Steel Moment-Resisting Frames Using Enhanced Vibrating Particles System Algorithm

Pedram Hosseini [1,*]; Fazeleh Sadat Lajevardi [2]; Seyed Rohollah Hoseini Vaez [3]

1.Assistant Professor, Faculty of Engineering, Mahallat Institute of Higher Education, Mahallat, Iran
2. M.Sc. Graduate, Department of Civil Engineering, Faculty of Engineering, University of Qom, Qom, Iran
3. Professor, Department of Civil Engineering, Faculty of Engineering, University of Qom, Qom, Iran
* Corresponding author: *p.hosseini@mahallat.ac.ir*

ARTICLE INFO

Article history:
Received: 01 March 2025
Revised: 14 July 2025
Accepted: 18 July 2025

Keywords:
Enhanced Vibrating Particles System;
Robust design optimization;
Uncertainty;
Steel moment resisting frame;
Monte Carlo simulation.

ABSTRACT

This study presents a robust design optimization (RDO) approach for 2D steel moment-resisting frames, addressing uncertainties in material properties and external loads. The study considers special moment frames with high ductility capacity (R=8) designed according to American Institute of Steel Construction Load and Resistance Factor Design (AISC-LRFD) specifications. The objective is to minimize both structural weight and the robustness index, defined as the standard deviation of roof displacement. The Enhanced Vibrating Particles System (EVPS) algorithm is employed to solve the optimization problem, while Monte Carlo simulation (MCS) is used to model uncertainties. Three benchmark frames (10, 15, and 24 stories) demonstrate the effectiveness of the proposed methodology. Results show a 50-60% reduction in roof displacement variability compared to deterministic optimization, with only a 20-30% increase in structural weight. For the 10-story frame with β=0.4, the approach achieved a 67% reduction in standard deviation (from 0.484 to 0.159) with a 74% weight increase (from 63,848 lb to 111,701 lb). The robustness index coefficient (β) is identified as a key parameter for controlling the weight-robustness trade-off, allowing designers to tailor solutions based on project requirements. The study provides a practical framework for improving steel frame reliability under real-world conditions.

E-ISSN: 2345-4423

How to cite this article:
Hosseini, P., Lajevardi, F. S. and Hoseini Vaez, S. R. (2026). Optimum Robust Design of 2D Steel Moment-Resisting Frames Using Enhanced Vibrating Particles System Algorithm. Journal of Rehabilitation in Civil Engineering, 14(2), 2284 http://doi.org/10.22075/jrce.2025.2284

1. Introduction

Structural optimization aims to achieve optimal designs satisfying constraints at minimum cost [1–4]. While gradient-based methods exist, metaheuristic algorithms such as genetic [5], bat [6], IPSO [7], ant colony [8], and WOA [9] are widely employed due to the absence of direct mathematical equations. Civil engineering applications utilize shape [10,11] and sizing [12] optimization to create cost-effective, material-efficient designs.

Recent advances have integrated optimization with sensitivity analysis techniques. Saldaña-Robles et al. [13] combined TA, FEA, RSM, and ANN for agricultural backhoe design, achieving 24.8% mass reduction. Sadeghpour and Ozay [14] compared ANN, RSM, and ANFIS for RC structure collapse potential assessment. Nouri et al. [15] integrated optimization and ANOVA for glass fiber polymer reinforcement. However, deterministic optimization neglects uncertainty despite safety factor slacking probabilistic basis [16]. Even 0.1% uncertainty can yield infeasible solutions [17], necessitating uncertainty consideration in design [18–21]. Recent reliability-based and robust design studies have advanced structural optimization [22]. Yadav and Ganguli [23] investigated uncertainty effects on trusses and composite plates. Dammak et al.[24] developed methods for acoustic-structural systems. Kamel et al. [25] optimized offshore wind turbines considering soil-structure interaction. Yarasca et al. [26] presented machine learning-optimized deformation theory for functionally graded plates. Two approaches handle uncertainty: RBDO models uncertainties probabilistically focusing on failure probability [27,28], while RDO emphasizes insensitivity to variation measured by response standard deviation [29].

Hosseini et al. [30] compared EVPS and GWO algorithms for steel frame RBDO, demonstrating weight reduction while maintaining reliability. The robustness concept, introduced by Taguchi [31,32], has been applied across engineering disciplines [33–39]. Early applications by Chi and Blöbaum [40] and Lee et al. [41] suffered from efficiency limitations. More effective approaches include Sandgren and Cameron's genetic algorithm with MCS [42] and Doltsinis and Kang's bi-criteria formulation [43]. Lagaros et al. [44] proposed multi-objective evolutionary methods, while Beyer and Sendhoff [45] reviewed robust optimization approaches. Recent advances include Zaman et al.'s [33] formulas for aleatory and epistemic uncertainties, Kan's [46] ellipsoid convex model, and Liu et al.'s [47] RDO of steel frames minimizing drift and weight. Zhao et al. [48] integrated RBDO with photovoltaic systems, Lyu et al. [49] developed non-iterative frameworks, Chen et al. [50] proposed quantile surrogates, and Steinacker et al. [51] investigated bicycle infrastructure robustness. Performance-based approaches by Saffari et al. [52], Bakhshinezhad et al. [53], and Roohbakhsh et al. [54] address uncertainty in seismic performance. Do and Ohsaki [55,56] formulated multi-objective RDO using Gaussian mixture models and Bayesian optimization. Zhang and Hu [57] optimized self-centering brace arrangements, while Soleymani et al. [58,59] investigated separation gaps and hybrid strong-back systems.

Despite these advances, comprehensive RDO investigations of high-rise steel moment frames remain limited. This study addresses this gap by: (1) proposing an integrated EVPS-MCS approach minimizing weight and response variability; (2) systematically evaluating the weight-robustness trade-off through β coefficient variation; (3) demonstrating effectiveness across three benchmark frames; and (4) establishing the EVPS algorithm's capability for complex robust optimization problems.

2. Monte carlo simulation method

MCS is a computational algorithm using random sampling for problems where deterministic solutions are infeasible. The method proves valuable for stochastic structural analysis with multiple uncertainty variables. The study considers uncertainties in: modulus of elasticity (E), shear modulus(G), external forces (P), yield stress (F_y), cross-sectional areas (A), torsion constant (J), moment of inertia (I), plastic section modulus (Z), and elastic section modulus (S). All variables follow normal distributions with COV of 10%

for external loads and 5% for other parameters. The approach first applies deterministic constraints using mean values, then performs probabilistic assessment for feasible designs. MCS with 2×10^5 samples evaluate statistical quantities efficiently [27]. Figure 1 presents the systematic robustness assessment approach.

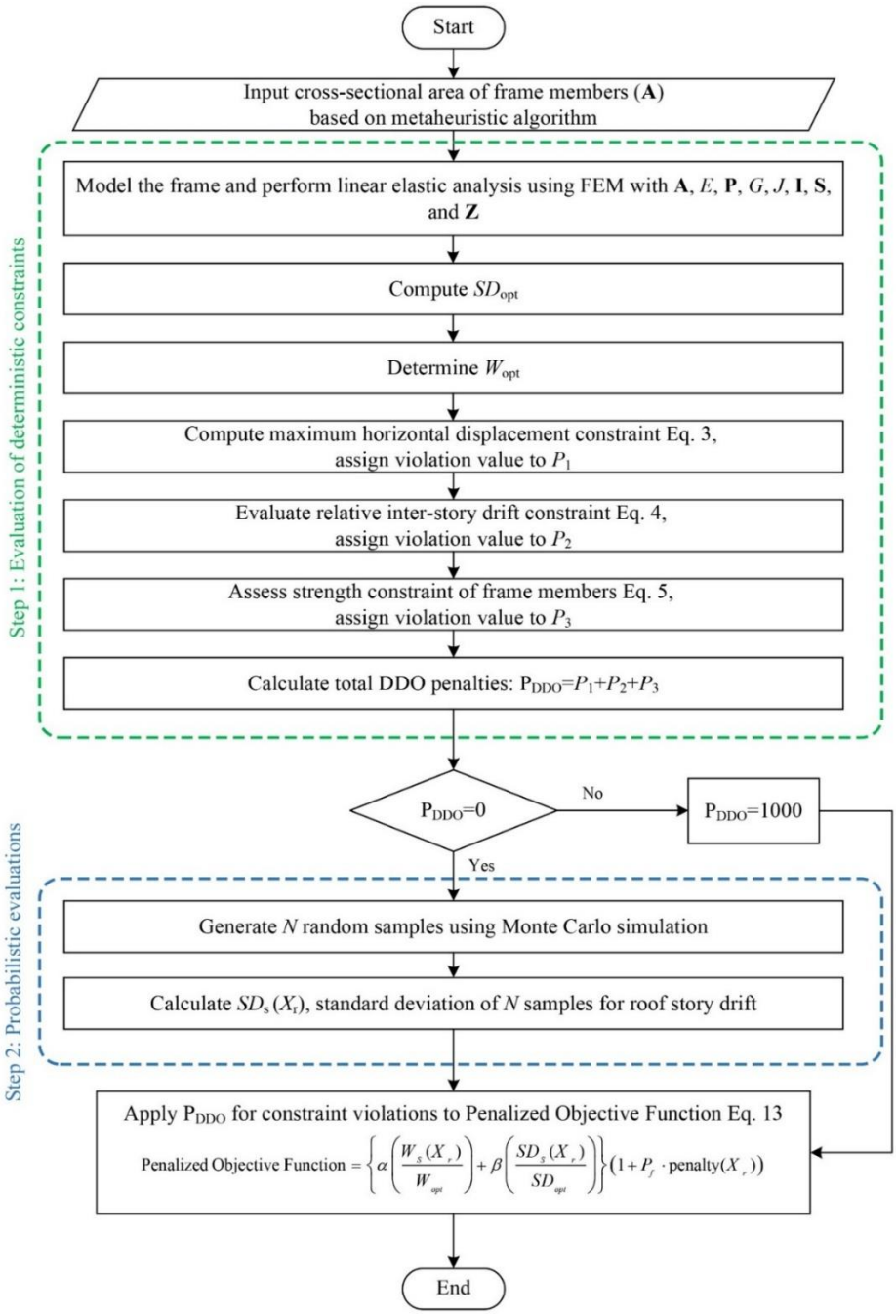

Fig. 1. Robustness response flowchart based on the Monte Carlo simulation method.

3. EVPS algorithm

The EVPS algorithm, inspired by single degree-of-freedom system vibration with viscous damping, enhances the VPS algorithm's convergence speed and search capabilities [60]. Key improvements include replacing the memory parameter with *HB* parameter, storing historically superior positions. The algorithm updates particle positions using three equations selected randomly, with boundary violations handled through harmony search [61]. Figure 2 illustrates the complete workflow, while Figure 3 presents the pseudocode. All implementations utilized MATLAB R2022a [62].

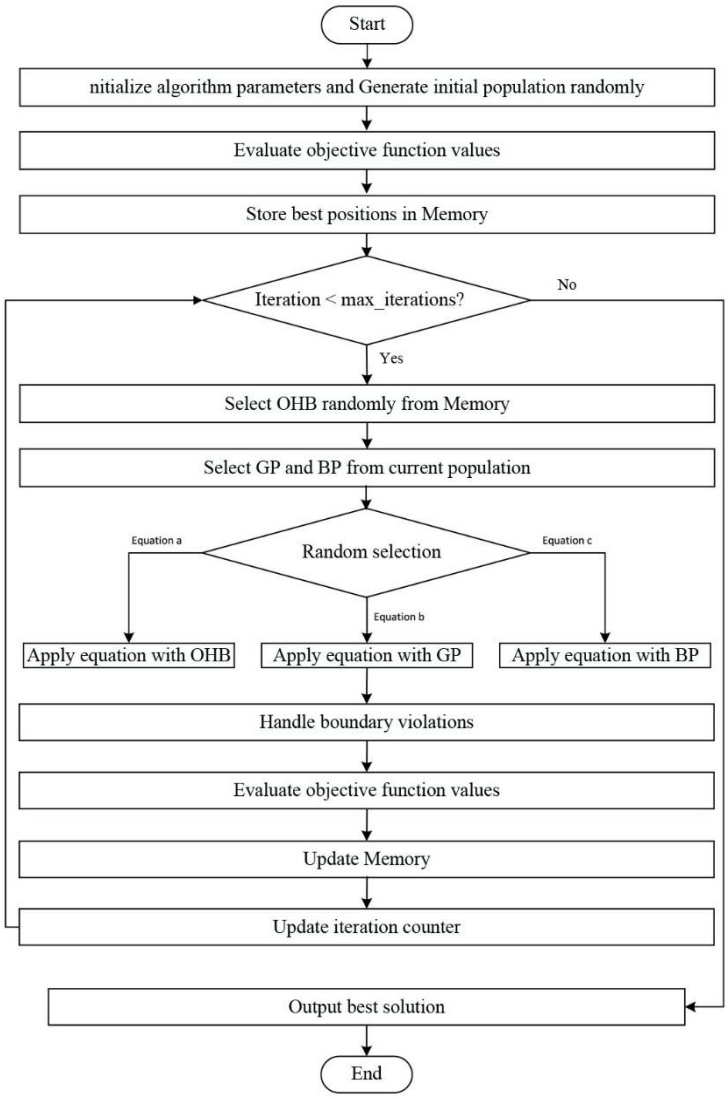

Fig. 2. Flowchart of the Enhanced Vibrating Particles System (EVPS) algorithm.

```
1.  Procedure EVPS(population_size, max_iterations, memory_size)
2.  // Initialization
3.  Initialize population X randomly within bounds
4.  Evaluate fitness of all particles
5.  Initialize Memory with best solutions from X
6.  for iter = 1 to max_iterations do
      a.  for each particle i in population do
            i.  Select OHB randomly from Memory
           ii.  Select GP and BP from current population
          iii.  for each dimension j do
           iv.  D = (iter/max_iterations)^(-α)  // Damping coefficient
            v.  // Randomly choose one equation:
           vi.  Randomly select equation_type from {a, b, c}
          vii.  if equation_type = a then
                    1.  X_new[i,j] = D·(±1)·(OHB[j] - X[i,j])·rand() + OHB[j]
         viii.  else if equation_type = b then
                    1.  X_new[i,j] = D·(±1)·(GP[j] - X[i,j])·rand() + GP[j]
           ix.  else  // equation_type = c
                    1.  X_new[i,j] = D·(±1)·(BP[j] - X[i,j])·rand() + BP[j]
            x.  end if
           xi.  // Handle boundary violations
          xii.  if X_new[i,j] outside bounds then
                    1.  Apply harmony search-based boundary handling
         xiii.  end if
          xiv.  end for
      b.  end for
      c.  Evaluate fitness of all particles in X_new
      d.  Update X with best solutions from X and X_new
      e.  Update Memory if current best is better than Memory worst
7.  end for
8.  return best solution from Memory
9.  End Procedure
```

Fig. 3. Pseudocode for Enhanced Vibrating Particles System (EVPS).

4. RDO formulation

4.1. Optimum design

The general form of the optimization mathematical problem is initially presented as:

$$\begin{cases} \text{Find} \quad X_o = [x_{o1}, x_{o2}, \dots, x_{oj}] \quad (x_L \le x \le x_R) \\ \text{Minimizing} \quad f(X_o) \\ \text{Subject to} \begin{cases} g_i(X_o) \le 0 \quad (i = 1,2, \dots, m) \\ l_k(X_o) = 0 \quad (k = 1,2, \dots, n) \end{cases} \end{cases} \tag{1}$$

This equation represents a general form of an optimization problem. The vector X_o contains the design variables specifically for optimization. The objective function $f(X_o)$ aims to be minimized subject to inequality constraints $g_i(X_o) \le 0$and equality constraints $l_k(X_o) = 0$. The variables $x_{o1}, x_{o2}, \dots, x_{oj}$ are bounded between x_L and x_R, representing the lower and upper limits respectively.

4.2. Structural optimization

In structural optimization, the objective is to minimize the weight of the structure while meeting the constraints of the regulations. The structural optimization formula is:

$$\begin{cases} \text{Find} \quad X_s = [x_{s1}, x_{s2}, x_{s3}, \dots, x_{sn_s}] \\ \text{To minimize} \quad w(X_s) = \sum_{i=1}^{m_s} \rho_i \, x_{si} L_i \\ \text{Subject to} \quad g_i(X_s) \le 0 \end{cases} \tag{2}$$

This equation is specific to structural optimization, where the goal is to minimize the weight of a structure while adhering to certain constraints. The vector X_s consists of design variables for structural parameters. The objective function $w(X_s)$ calculates the total weight of the structure, using the material density ρ_i, lengths L_i, and design variables x_{si}. The constraints $g_i(X_s) \le 0$ ensure the structure meets regulatory requirements.

The design variables encompass structural parameters, encompassing dimensions, shape, and topology. Objectives and constraints typically encompass structural weight, static and transient responses. These constraints encompass the following:

According to LRFD-AISC [63], the constraints include force and displacement where:

- The constraint related to maximum horizontal displacement of the structure is:

$$\frac{\Delta_T}{H} - R \le 0 \tag{3}$$

- The constraint associated with the relative inter-story drift is:

$$\frac{|d_i|}{h_i} - R_l \le 0; i = 1,2, \dots, ns \tag{4}$$

- The strength constraint of the frame members or strength is the simultaneous effect of the bending moment and axial compressive force as:

$$\frac{P_u}{2\phi_c P_n} + \left[\frac{M_{ux}}{\phi_b M_{nx}} + \frac{M_{uy}}{\phi_b M_{ny}}\right] - 1 \le 0; for \frac{P_u}{\phi_c P_n} \le 0.2 \quad \frac{P_u}{\phi_c P_n} + \frac{8}{9}\left[\frac{M_{ux}}{\phi_b M_{nx}} + \frac{M_{uy}}{\phi_b M_{ny}}\right] - 1 \le 0; for \frac{P_u}{\phi_c P_n} \ge 0.2 \tag{5}$$

In equation (3), Δ_T and H denote the maximum horizontal displacement of the roof and the frame height, respectively, R denotes the maximum index of lateral displacement (1/300 in the present study). In equation (4), d_i and h_i denote the relative inter-story drift and the height of the desired story, respectively and R_i denotes the lateral displacement and is defined as R. In equation (5), P_n denotes the axial strength of the tensile or compressive members, $\emptyset_c$ denotes the axial strength-reduction factor (0.9 for tensile members and 0.85 for compressive members), M_u and M_n are the required and nominal flexural capacities, respectively, and $\emptyset_b$ is equal to the bending strength-reduction factor (0.9).

In equation (5), the axial strength of the members has been calculated as:

- For nominal strength of tensile members as:

$$P_n = A_g F_y \tag{6}$$

- For nominal strength of compressive members as:

$$P_n = A_g F_{cr} \tag{7}$$

$$F_{cr} = \left[0.658^{\lambda_c^2}\right] F_y; for \lambda_c \leq 1.5$$
$$F_{cr} = \left[\frac{0.877}{\lambda_c^2}\right] F_y; for \lambda_c > 1.5 \tag{8}$$

$$\lambda_c = \frac{kl}{r\pi}\sqrt{\frac{F_y}{E}} \tag{9}$$

In equations (6) and (7), A_g is equal to the cross-section of the members. In equation (9), k denotes the effective length factor, which equals 1 for the lateral braced length and is calculated for the lateral unbraced length as:

$$k = \sqrt{\frac{1.6G_AG_B+4.0(G_A+G_B)+7.5}{G_A+G_B+7.5}} \tag{10}$$

where G_A and G_B denote the boundary conditions of the two ends of the compressive member and depend on the $E1/L$ ratio of the columns and the sum of the same coefficient for the beam leading to the two ends of the compressive member.

The random structural parameters lead to performance dispersion as defined by the constraints, as a result of which robust design is required. The current study has expanded the deterministic optimal design problem for steel frames by considering the robustness of the responses. In other words, the objective is to minimize the structural weight and robustness index in addition to meeting specific design constraints.

4.3. Robust design

The RDO formulation used in the present study is derived through a series of equations, culminating in the final form presented in Equation (13). The process begins with the objective function of Equation (2), which is then expanded and modified to incorporate robustness considerations. The intermediate steps are represented by Equations (11) and (12), which introduce the robustness index and the trade-off between weight and robustness, respectively. Finally, the penalty terms are added in Equation (13) to ensure compliance with design constraints, resulting in the comprehensive RDO formulation employed in this research.

$$\begin{cases} \text{Find} \quad X_r = [x_{r1}, \dots, x_{rng}] \quad x_{ri} \in S_i \\ \text{To minimize} \quad \text{Robustness index}(X_r) \\ \text{Subjected to} \quad g_j(X_r) \leq 0, \quad \left[j = 1,2, \dots, nc_r; x_{i_{\min}} \leq x_{ri} \leq x_{i_{\max}}\right] \end{cases} \tag{11}$$

This formula is used in robust optimum design, which focuses on both minimizing structural weight and achieving a low robustness index. The vector X_r represents design variables related to robust design. The goal is to minimize the robustness index, which is a measure of the structure's performance variability. The constraints $g_j(X_r) \leq 0$ and $x_{i_{\min}} \leq x_{\mathrm{ri}} \leq x_{i_{\max}}$ ensure the design stays within acceptable limits while optimizing for both weight and robustness.

$$\text{Objective Function} = \alpha\left(\frac{W_S(X_r)}{W_{opt}}\right) + \beta\left(\frac{SD_S(X_r)}{SD_{opt}}\right) \tag{12}$$

In this context, $W_S(X_r)$ represents the structural weight associated with the design variables in X_r. W_{opt} stands for the optimal weight, which is determined irrespective of the robustness index considerations. Similarly, $SD_S(X_r)$ corresponds to the structural standard deviation linked to the design variables in X_r,

while SD_{opt} denotes an optimized standard deviation, established independently of structural weight considerations. where α and β respectively represent the coefficients for structural weight and robustness index This objective function effectively balances the trade-off between minimizing structural weight and standard deviation.

Accounting for the penalty effect, equation 12 is reformulated as equation 13:

$$\text{PenalizedObjective Function} = \left\{\alpha\left(\frac{W_S(X_r)}{W_{opt}}\right) + \beta\left(\frac{SD_S(X_r)}{SD_{opt}}\right)\right\}\left(1 + P_f \cdot \text{penalty}(X_r)\right) \quad (13)$$

Within this equation, P_f denotes the penalty coefficient. The study focuses on the displacement robustness index of the roof node. The objective, as articulated in equation (12), centers on the simultaneous minimization of both weight and robustness index while adhering to the constraints of the problem. The additional term $(1 + P_f \cdot \text{penalty}(X_r))$ in equation (13) accounts for the penalty effect, ensuring compliance with design requirements and constraints.

The study focuses on the displacement robustness index of the roof node. The objective, as articulated in Equation (12), centers on the simultaneous minimization of both weight and robustness index while adhering to the constraints of the problem. The additional terms in Equation (13) account for the penalty effect, ensuring compliance with design requirements and constraints.

5. Design examples

Three benchmark frames were optimized using EVPS with population size 60, 300 iterations, and parameters: w1=0.2, w2=0.3, HMCR=0.95, PAR=0.1, memory size=4. Table 1 presents uniform specifications facilitating direct comparison. MCS employed 2×10^5 samples considering 5% and10% COV for material properties and loads respectively.

Table 1. Uniform specifications of the benchmark steel frames.

Parameter	10-Story Frame	15-Story Frame	24-Story Frame
Geometric Properties			
Number of stories	10	15	24
Number of bays	1	3	3
Total height(m)	37.4904	53	87.6
Story height(m)	4.572+9@3.6576	4+14@3.5	3.65
Bay width(m)	9.144	3@5	6.09+3.65+8.53
Number of nodes	11	64	100
Number of members	30	105	168
Design Variables			
Total design variable groups	9	11	20
Column groups	5	10	16
Beam groups	4	1	4
Material Properties			
Modulus of elasticity (*E*) (GPa)	200	200	205
Yield stress (F_y) (MPa)	248.2	248.2	230.28
Effective Length Factors			
kx (in-plane)	≥ 1	≥ 0	≥ 1
ky (out-of-plane)	1.0	1.0	1.0
Section Database			
Column sections	W12 and W14 sections	267 W-shaped sections	W14 sections
Beam sections	267 W-shaped sections	267 W-shaped sections	267 W-shaped sections
Design Constraints			
Primary constraint	AISC-LRFD strength & drift	AISC-LRFD strength & drift	AISC-LRFD strength & drift
Drift limit	1/300 of height	1/300 of height	1/300 of height
Unbraced Length			
Columns	Full height	Full height	Full height
Beams	1/5 of bay length	1/5 of bay length	Full length
Reference	[64]	[64]	[64]

5.1. 10-story single-bay frame

The 10-story frame (Figure 4) contains 11 nodes and 30 members with nine design variable groups. Specifications are detailed in Table 1. Table 2 presents optimal solutions for varying β values, demonstrating increased weight but decreased standard deviation with higher β.

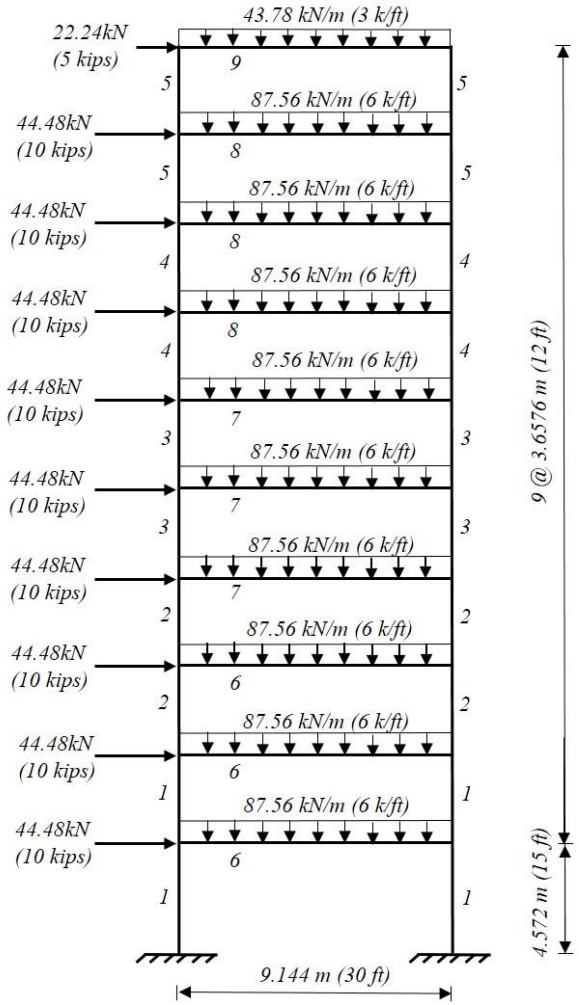

Fig. 4. Schematic of a single-bay 10-story frame [64].

Table 2. Optimal solutions for the one-bay, 10-story frame using EVPS with different β values.

	EVPS (DDO+RDO)			EVPS(DDO)[64]	SDE(DDO) [64]
	Alpha=1			Alpha=1	Alpha=1
Group	Betta=0.2	Betta=0.4	Betta=0.6	Betta=0	Betta=0
1	W14x283	W14x426	W14x500	W14x233	W14x233
2	W14x233	W14x283	W14x370	W14x176	W14x176
3	W14x193	W14x193	W14x257	W14x159	W14x145
4	W14x99	W14x159	W14x233	W14x99	W14x99
5	W14x53	W14x68	W14x109	W14x61	W12x65
6	W40x167	W44x230	W44x290	W33x118	W33x118
7	W40x167	W40x215	W44x262	W30x90	W30x99
8	W36x135	W40x149	W40x167	W27x84	W27x84
9	W24x68	W18x46	W21x55	W18x46	W21x44
best weight	39656.859 kg (87428.40942 lb)	50666.53 kg (111700.5794 lb)	63609.169 kg (140234.2131 lb)	28960.918 kg (63847.8970 lb)	29194.474 kg (64362.7994 lb)
standard deviation	0.23230368	0.158962123	0.116392685	0.484314	0.479565

Figures 5-12 illustrate the β coefficient effects, convergence curves, stress ratios, inter-story drift, roof displacement, and Monte Carlo results. The stress distribution shows more uniform patterns in robust designs, with maximum ratios below 0.85 providing uncertainty buffer. Density plots confirm narrower displacement distributions with increasing β.

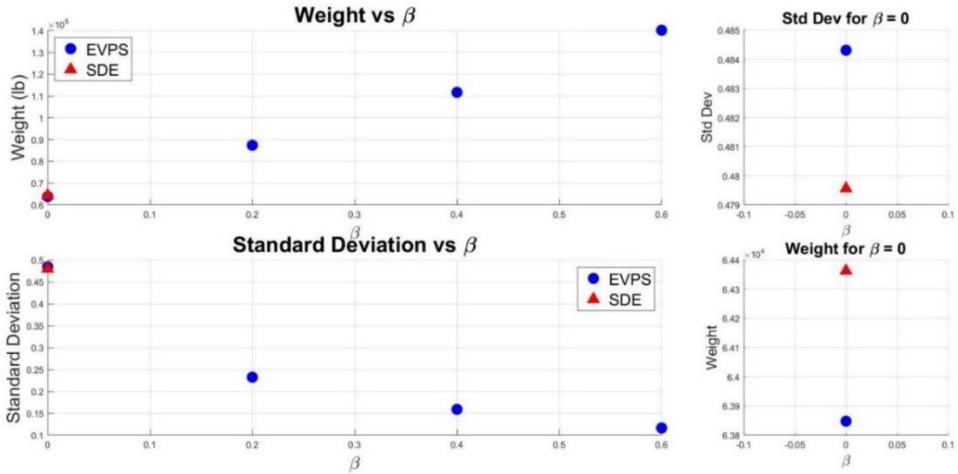

Fig. 5. Effect of $\boldsymbol{\beta}$ coefficient on weight and standard deviation of a 10-story, single-bay frame structure.

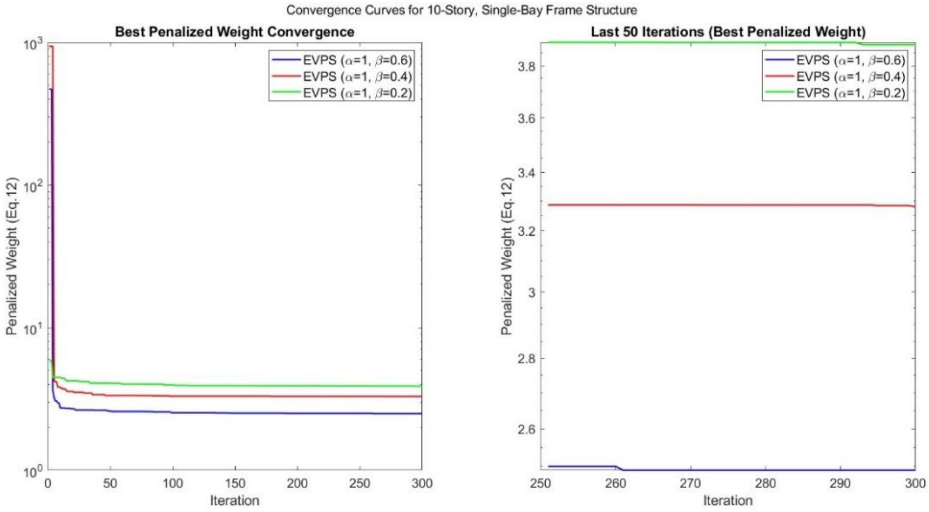

Fig. 6. Convergence curves for the 10-story, single-bay frame structure.

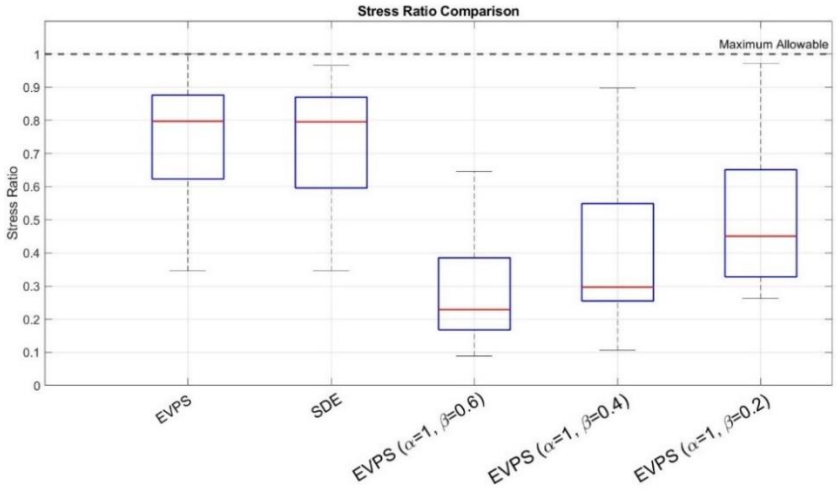

Fig. 7. Stress ratio chart for different design cases of the 10-story, single-bay frame structure.

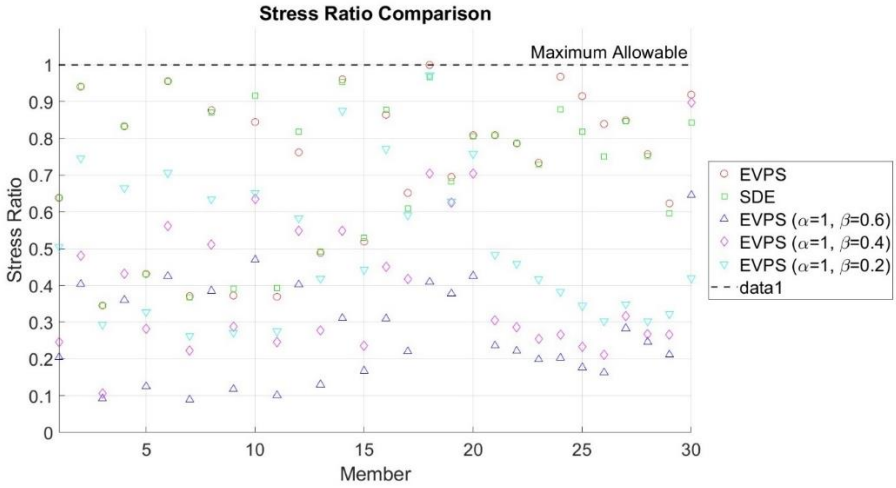

Fig. 8. Stress ratio scatter plot for different design cases of the 10-story, single-bay frame structure.

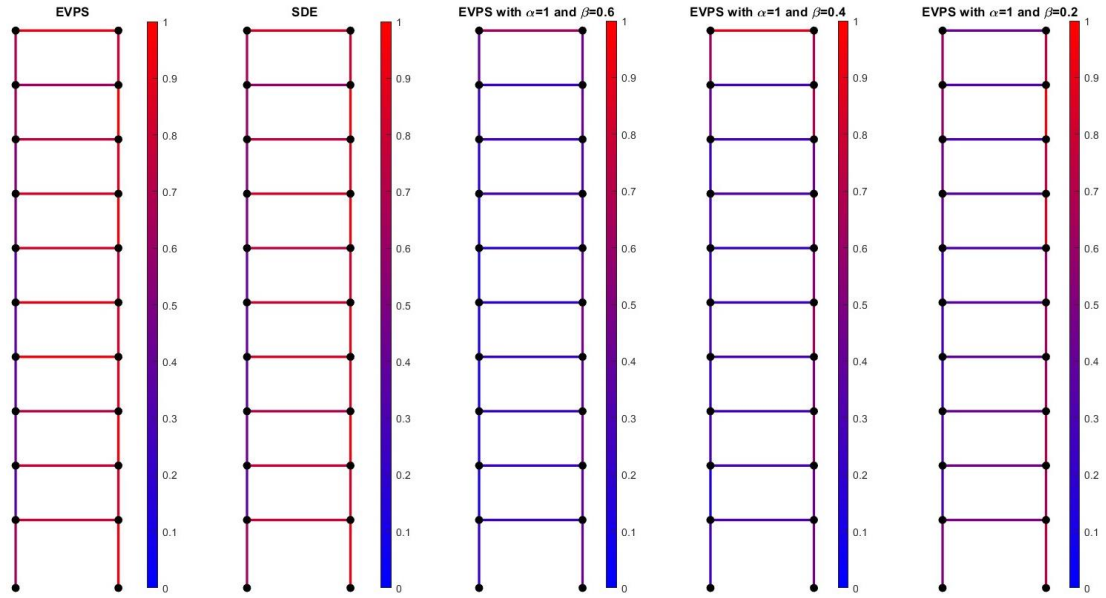

Fig. 9. Stress ratio contour plot for different design cases of the 10-story, single-bay frame structure.

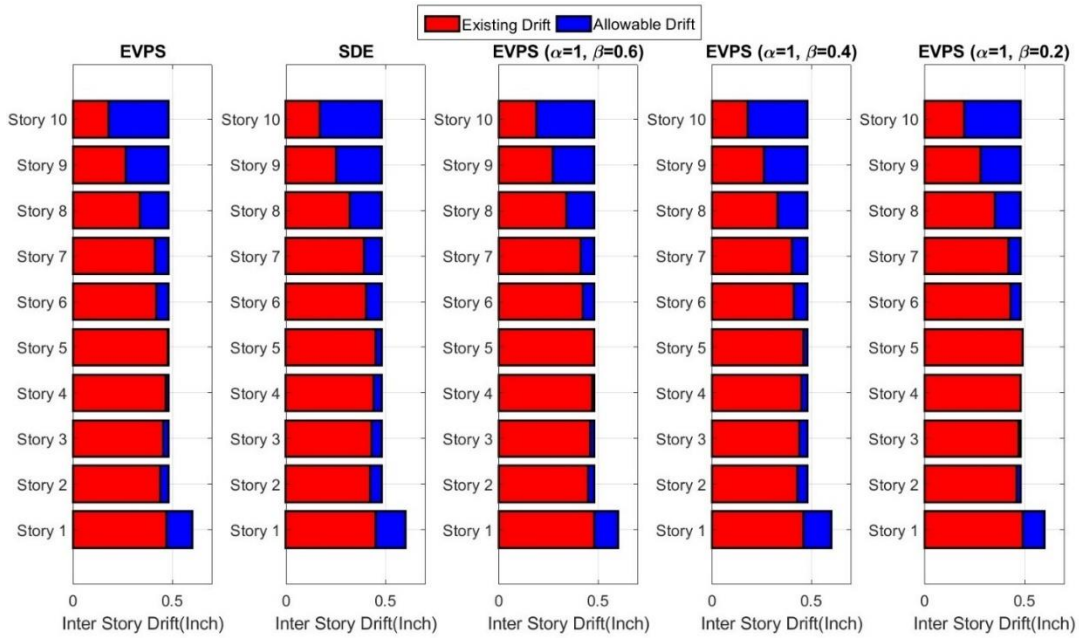

Fig. 10. Inter-story drift plot for different design cases of the 10-story, single-bay frame structure.

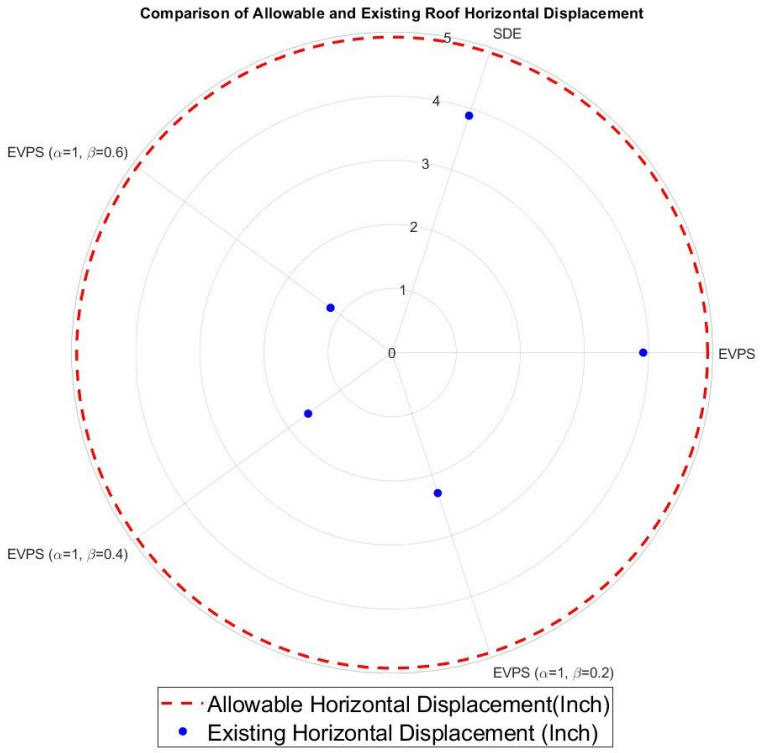

Fig. 11. Roof horizontal displacement comparison plot for different design cases of the 10-story, single-bay frame structure.

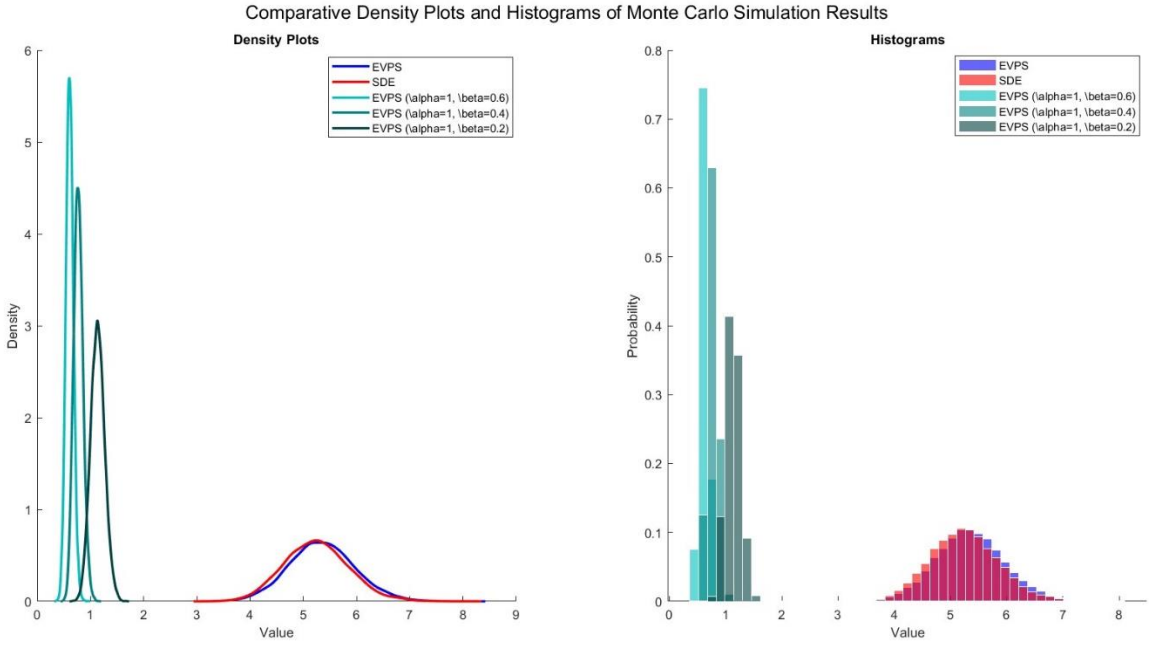

*Horizontal axis: Roof Displacement (mm); Vertical axis: Probability Density of Roof Displacement Distribution from Monte Carlo

Fig. 12. Comparative density plots and histograms of Monte Carlo simulation results for different design cases of the 10-story, single-bay frame structure.

5.2. 15-story frame

The 15-story three-bay frame (Figure 13) contains 64 nodes and 105 members with 11 design groups (specifications in Table 1). Table 3 presents optimization results showing similar weight-robustness trade-offs.

Table 3. Optimal solutions for the three-bay, 15-story frame using EVPS with different β values.

	EVPS (DDO+RDO)			EVPS(DDO) [64]	SDE(DDO) [64]
		Alpha=1		Alpha=1	Alpha=1
Group	Betta=0.2	Betta=0.4	Betta=0.6	Betta=0	Betta=0
1	W40x249	W44x335	W40x503	W14x99	W14x90
2	W40x149	W40x215	W40x199	W27x161	W36x170
3	W36x182	W44x290	W36x359	W27x84	W27x84
4	W40x149	W40x183	W36x150	W24x104	W24x104
5	W27x102	W36x150	W36x182	W14x61	W14x61
6	W33x118	W40x167	W40x149	W30x90	W30x90
7	W30x90	W30x108	W36x135	W14x48	W14x48
8	W30x90	W40x167	W33x118	W12x65	W12x65
9	W14x34	W24x55	W30x99	W6x25	W6x25
10	W27x94	W30x124	W36x135	W12x40	W12x40
11	W33x118	W36x135	W40x167	W21x44	W21x44
best weight	79486.948 kg (175238.7238 lb)	102306.861 kg (225548.0217 lb)	120582.928 kg (265839.8512 lb)	39553.772 kg (87201.1409 lb)	39528.279 kg (87144.9387 lb)
standard deviation	0.129005855	0.087387483	0.068182942	0.256002332	0.272184862

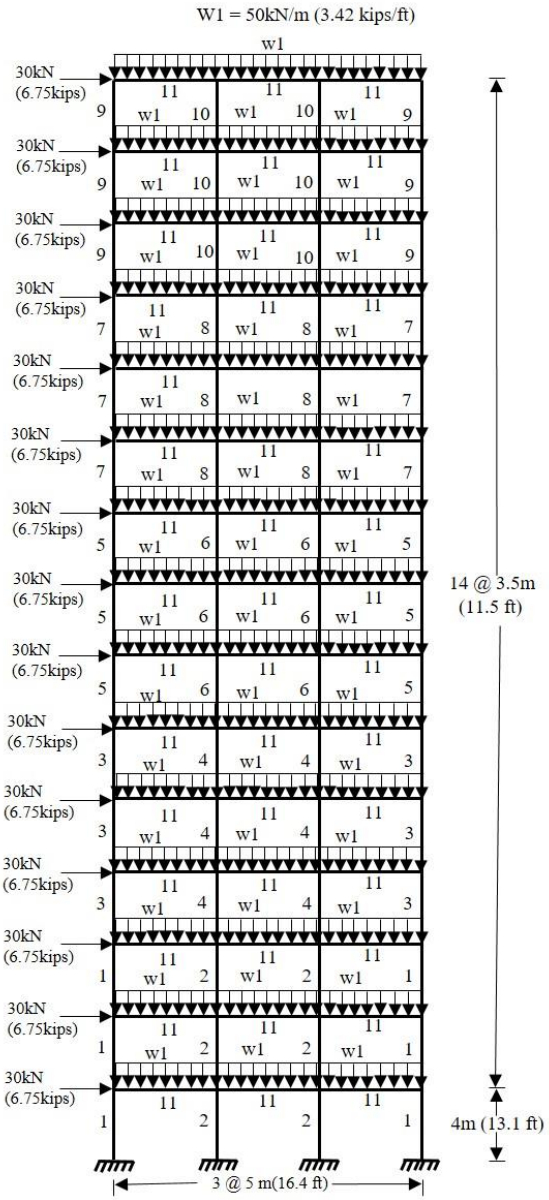

Fig. 13. Schematic of a three-bay 15-story frame [64].

Figures 14-21 demonstrate β effects, convergence, stress distributions, drift profiles, and Montecarlo results, confirming robust design effectiveness for multi-bay configurations.

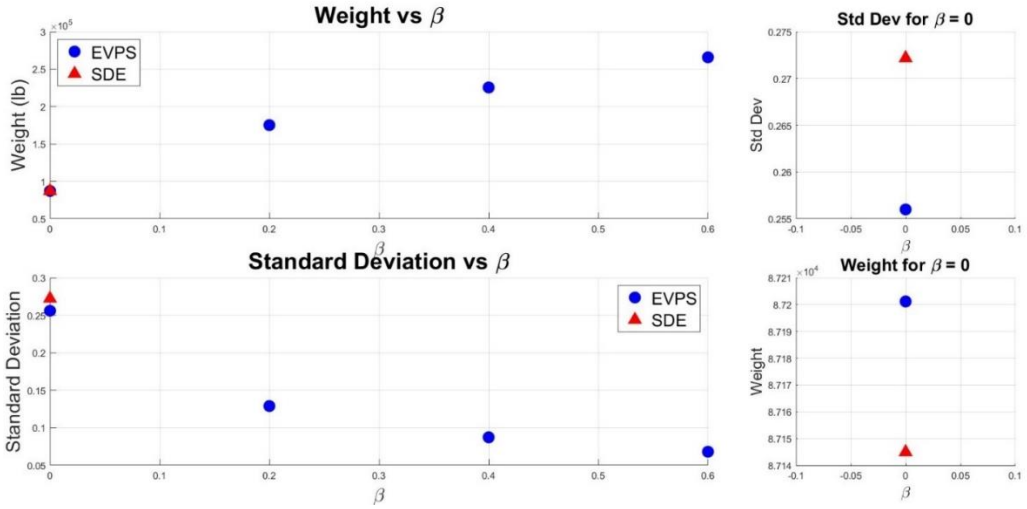

Fig. 14. Effect of $\boldsymbol{\beta}$ coefficient on weight and standard deviation of a three-bay 15-story frame.

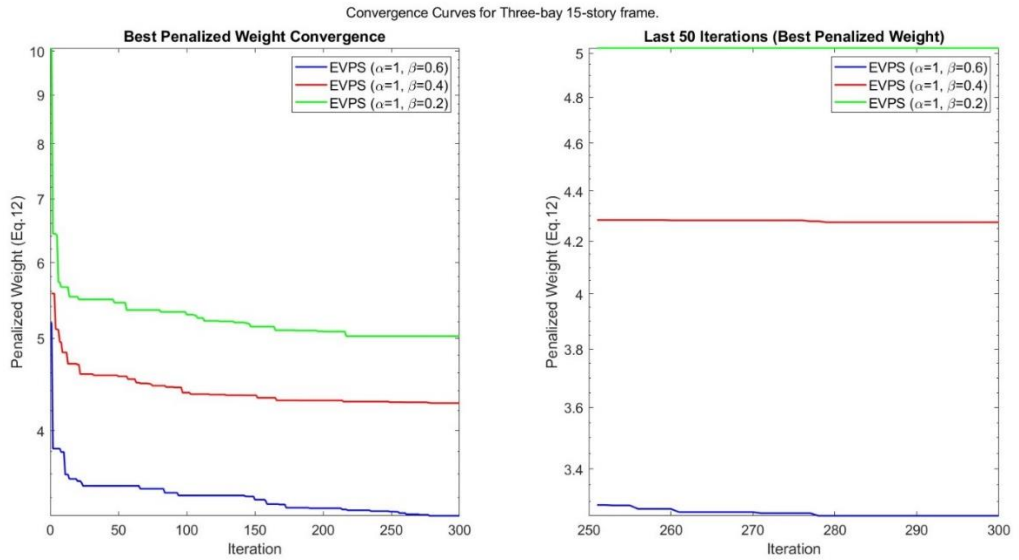

Fig. 15. Convergence curves for the three-bay 15-story frame.

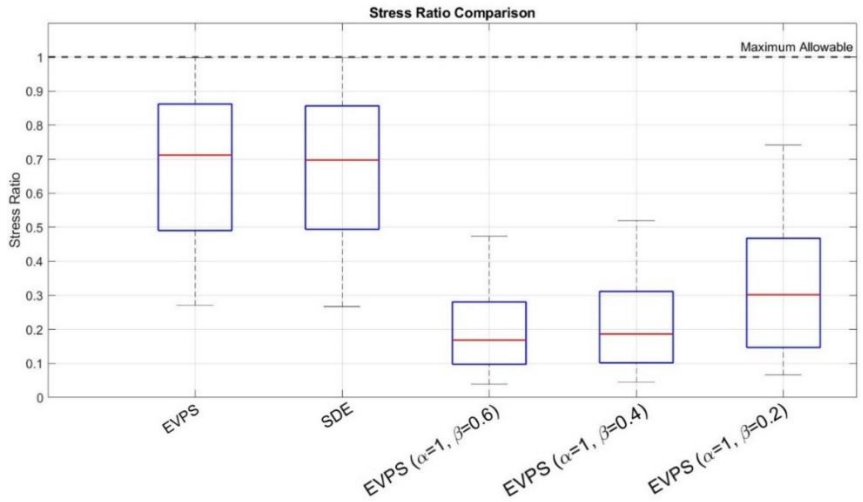

Fig. 16. Stress ratio chart for different design cases of the three-bay 15-story frame.

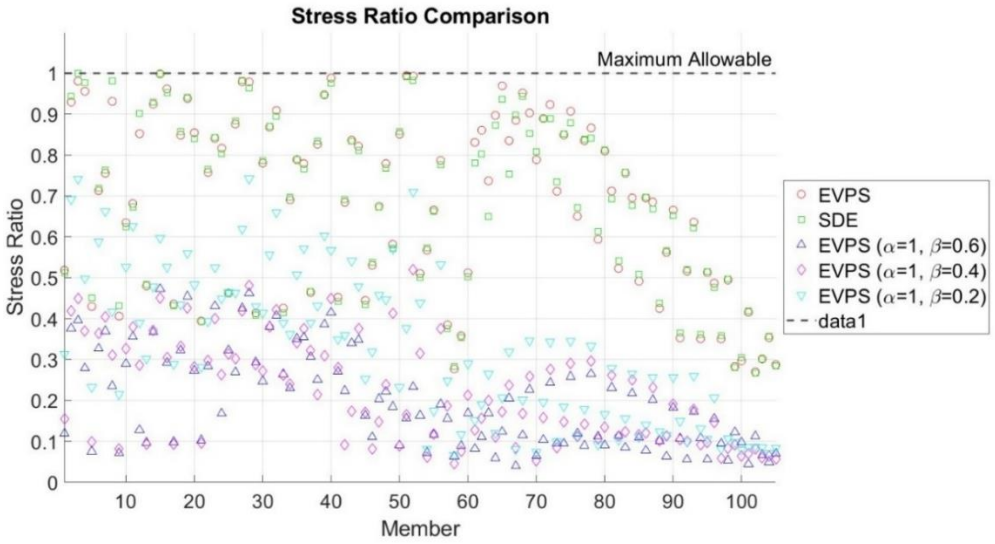

Fig. 17. Stress ratio scatter plot for different design cases of the three-bay 15-story frame.

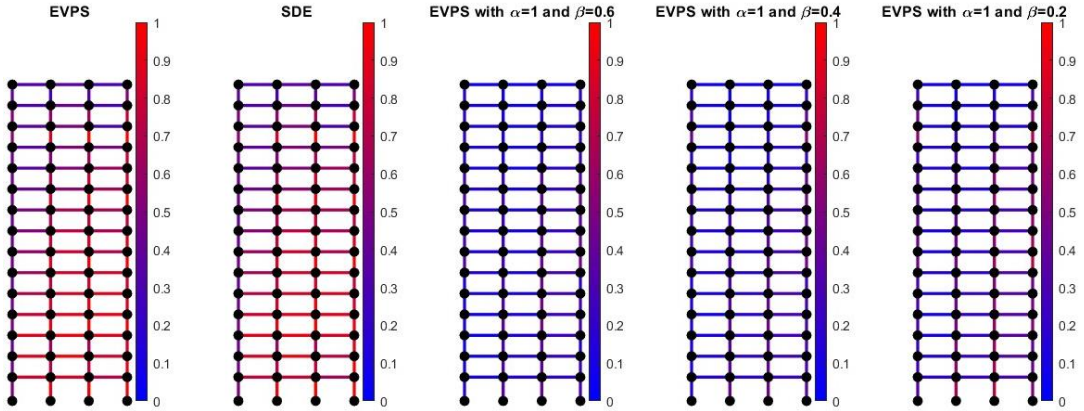

Fig. 18. Stress ratio contour plot for different design cases of the three-bay 15-story frame.

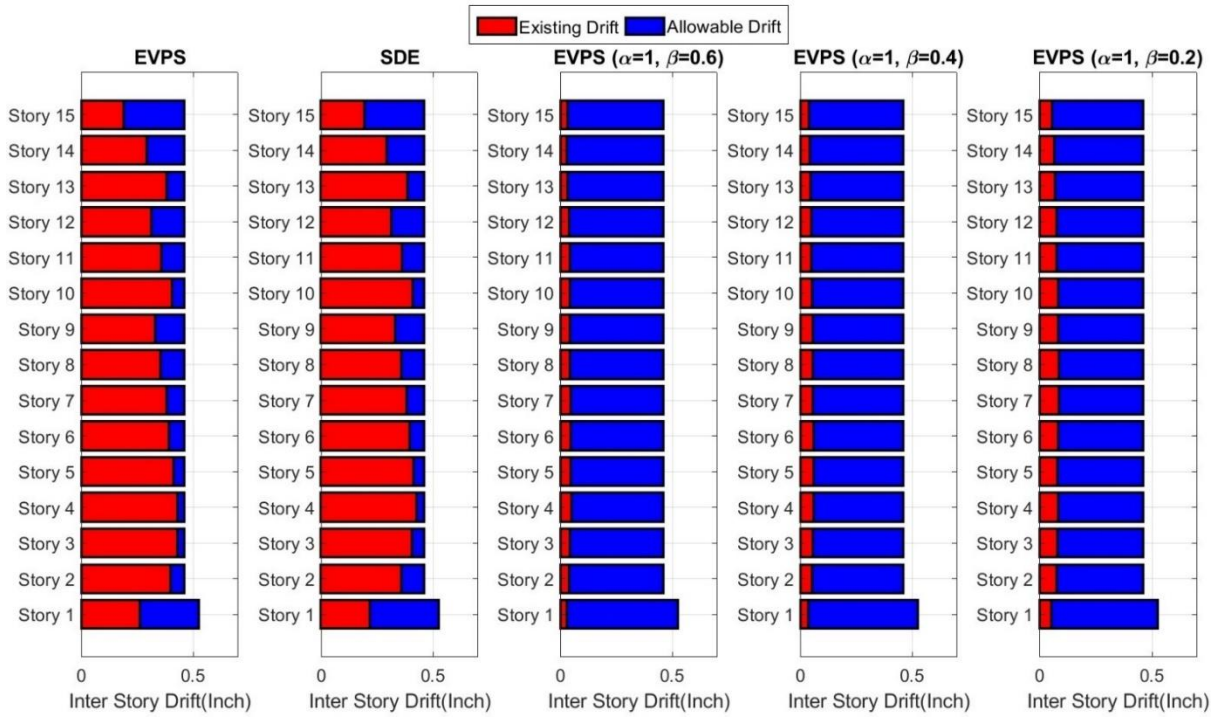

Fig. 19. Inter-story drift plot for different design cases of the three-bay 15-story frame.

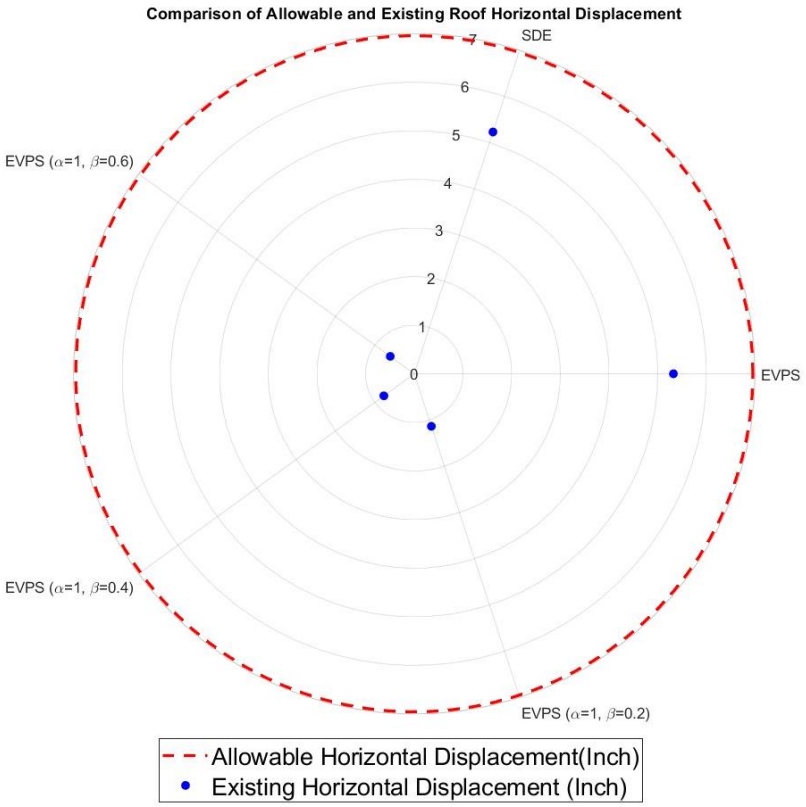

Fig. 20. Roof horizontal displacement comparison plot for different design cases of the three-bay 15-story frame.

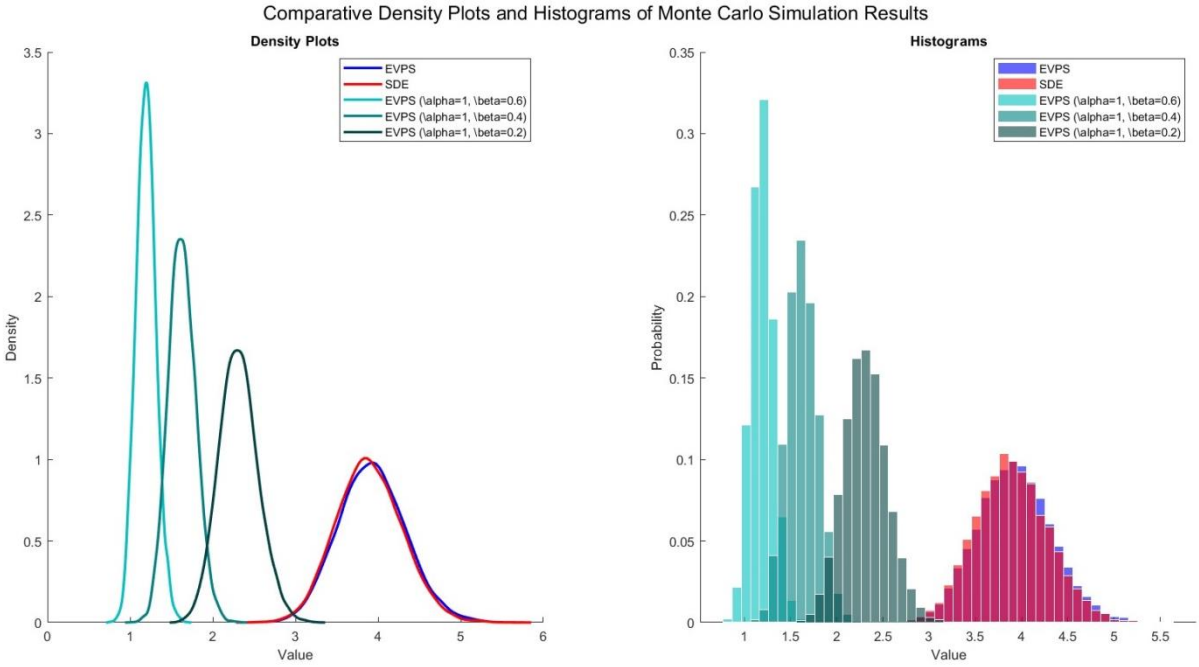

*Horizontal axis: Roof Displacement (mm); Vertical axis: Probability Density of Roof Displacement Distribution from Monte Carlo

Fig. 21. Comparative density plots and histograms of Monte Carlo simulation results for different design cases of the three-bay 15-story frame.

5.3. 24-story frame

The 24-story frame (Figure 22) contains 100 nodes and 168 members with 20 design groups (specifications in Table 1). Table 4 shows optimization results.

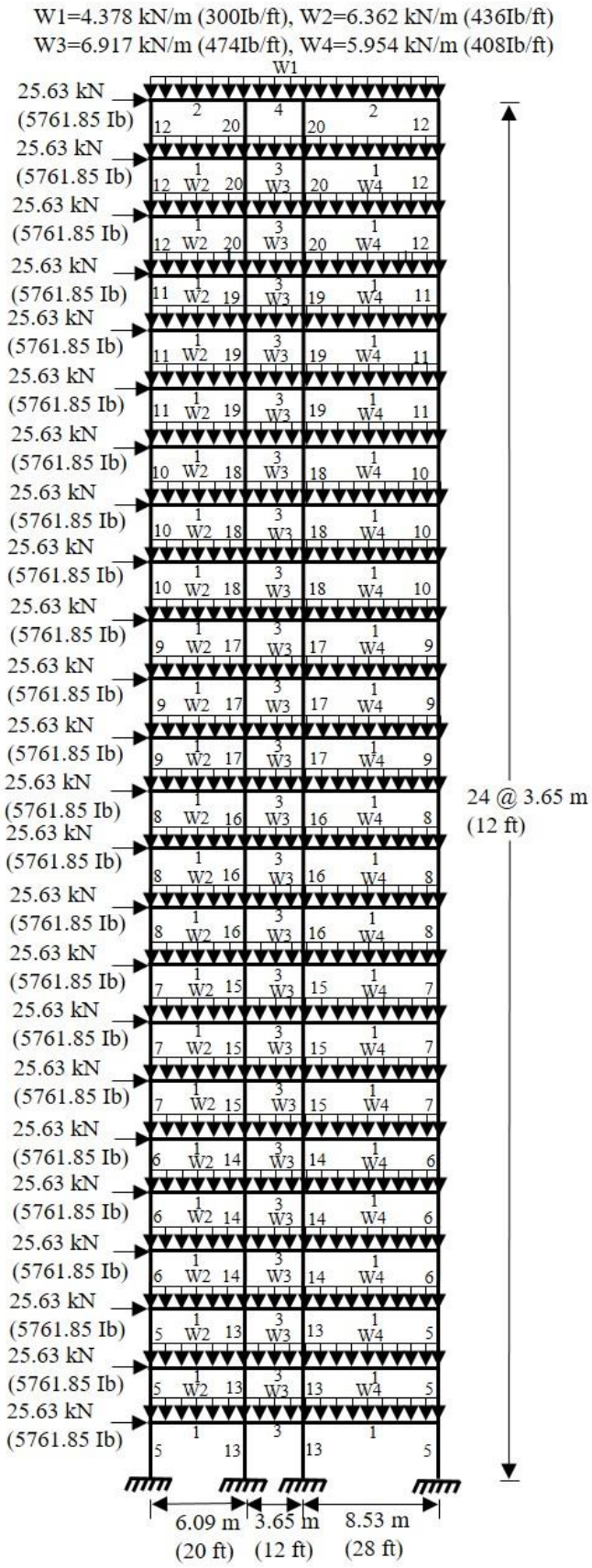

Fig. 22. Schematic of a three-bay 24-story frame [64].

Figures 23-30 present comprehensive results demonstrating the methodology's scalability to high-rise structures, with consistent weight-robustness relationships.

Table 4. Optimal solutions for the three-bay, 24-story frame using EVPS with different β values..

	EVPS (DDO+RDO)			EVPS(DDO) [64]	SDE(DDO) [64]
Group	Betta=0.2	Alpha=1 Betta=0.4	Betta=0.6	Alpha=1 Betta=0	Alpha=1 Betta=0
1	W33x118	W40x149	W40x183	W30x90	W30x90
2	W14x38	W14x43	W12x50	W6x15	W6x15
3	W27x84	W27x114	W33x118	W24x55	W24x55
4	W16x89	W24x62	W24x84	W6x8.5	W6x8.5
5	W12x79	W14x99	W14x120	W14x159	W14x159
6	W12x72	W14x82	W12x96	W14x145	W14x132
7	W12x65	W12x79	W12x96	W14x90	W14x109
8	W12x65	W12x72	W12x87	W14x74	W14x74
9	W14x53	W14x61	W14x74	W14x74	W14x61
10	W14x43	W12x50	W14x61	W14x38	W14x38
11	W12x45	W12x40	W12x45	W14x30	W14x34
12	W12x40	W12x35	W12x35	W14x22	W14x22
13	W14x61	W14x61	W14x74	W14x99	W14x90
14	W12x65	W12x65	W14x74	W14x90	W14x99
15	W14x48	W12x72	W14x74	W14x99	W14x90
16	W12x53	W12x72	W12x65	W14x90	W14x90
17	W14x43	W12x50	W14x68	W14x68	W14x74
18	W14x43	W12x65	W12x58	W14x61	W14x61
19	W14x38	W14x43	W12x53	W14x43	W14x34
20	W12x30	W12x35	W14x53	W14x22	W14x22
best weight	151002.308 kg (332903.1045 lb)	197691.642 kg (435835.4673 lb)	247166.409 kg (544908.6581 lb)	91663.310 kg (202083.0070 lb)	91175.885 kg (201008.4202 lb)
standard deviation	0.573059761	0.39000903	0.28992228	1.177252288	1.198756896

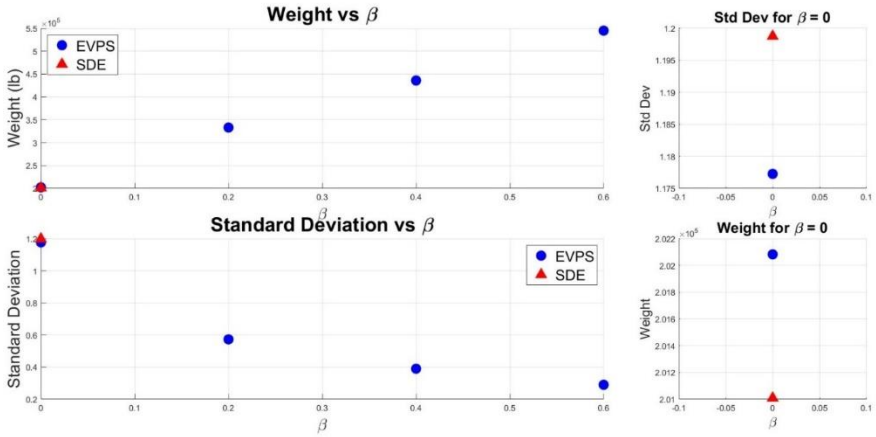

Fig. 23. Effect of β coefficient on weight and standard deviation of a three-bay 24-story frame.

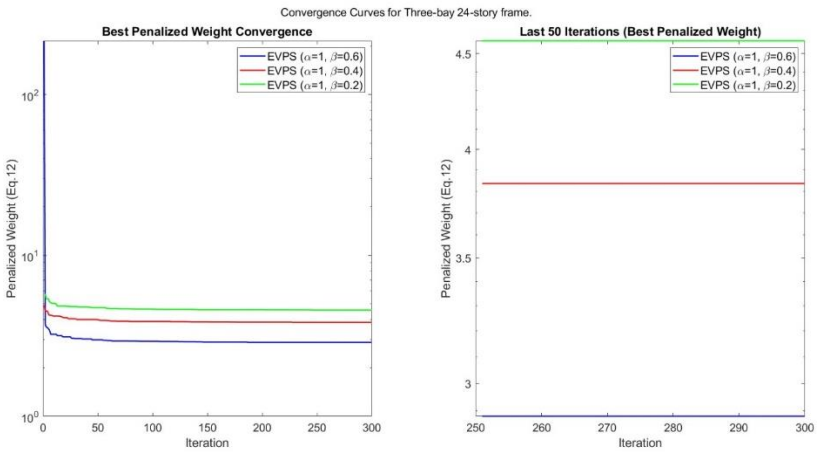

Fig. 24. Convergence curves for the three-bay 24-story frame.

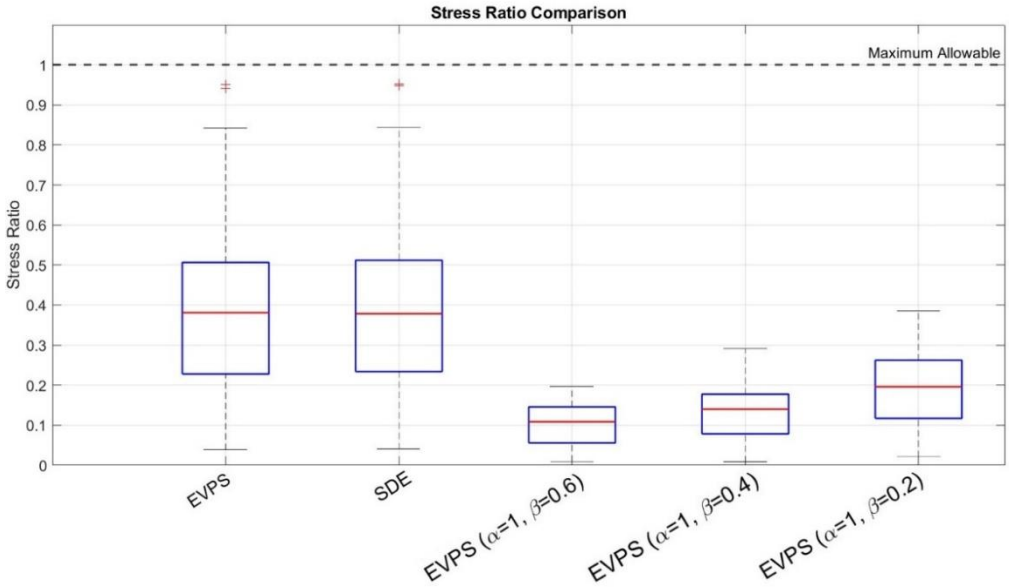

Fig. 25. Stress ratio chart for different design cases of the three-bay 24-story frame.

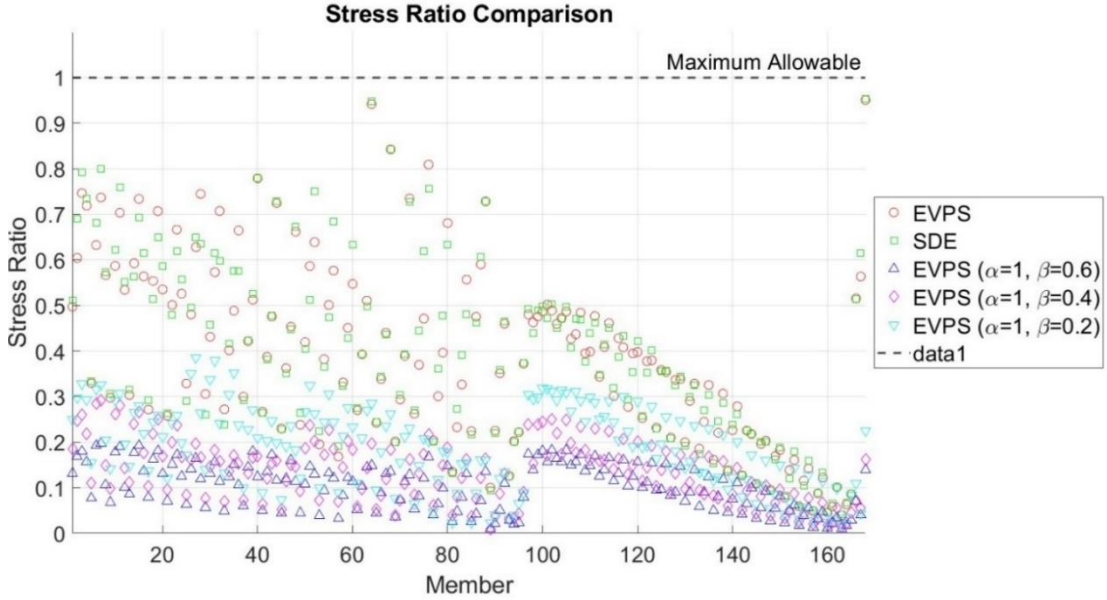

Fig. 26. Stress ratio scatter plot for different design cases of the three-bay 24-story frame.

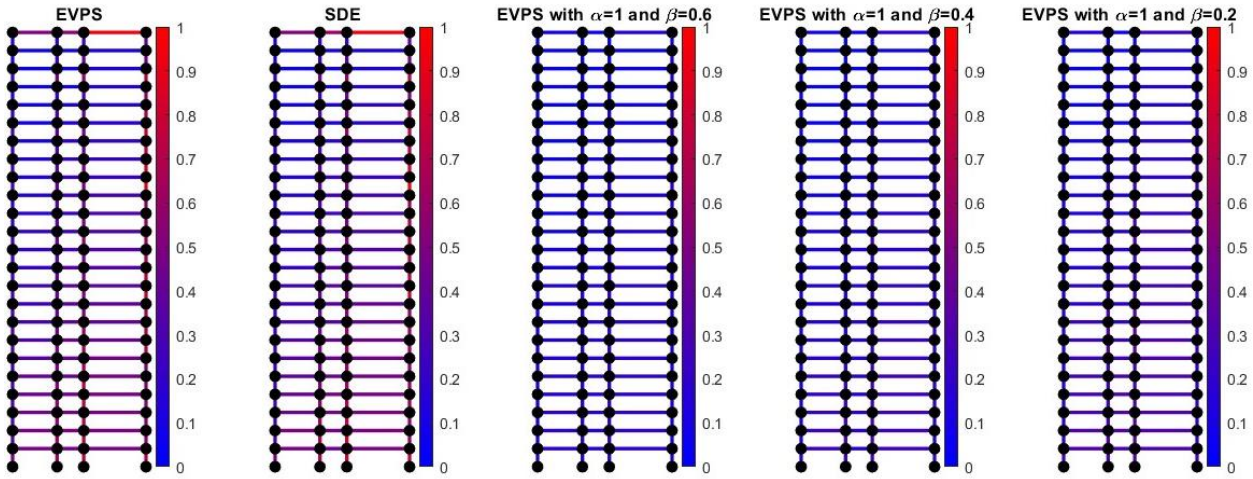

Fig. 27. Stress ratio contour plot for different design cases of the three-bay 24-story frame.

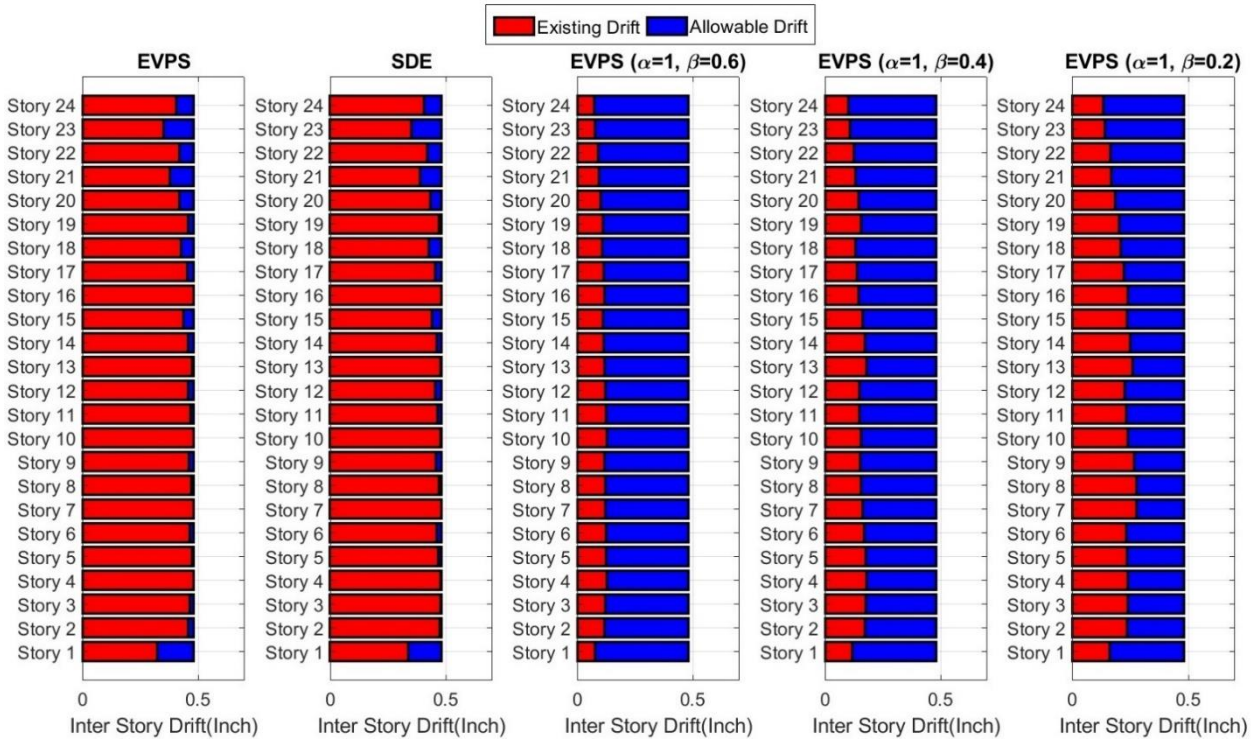

Fig. 28. Inter-story drift plot for different design cases of the three-bay 24-story frame.

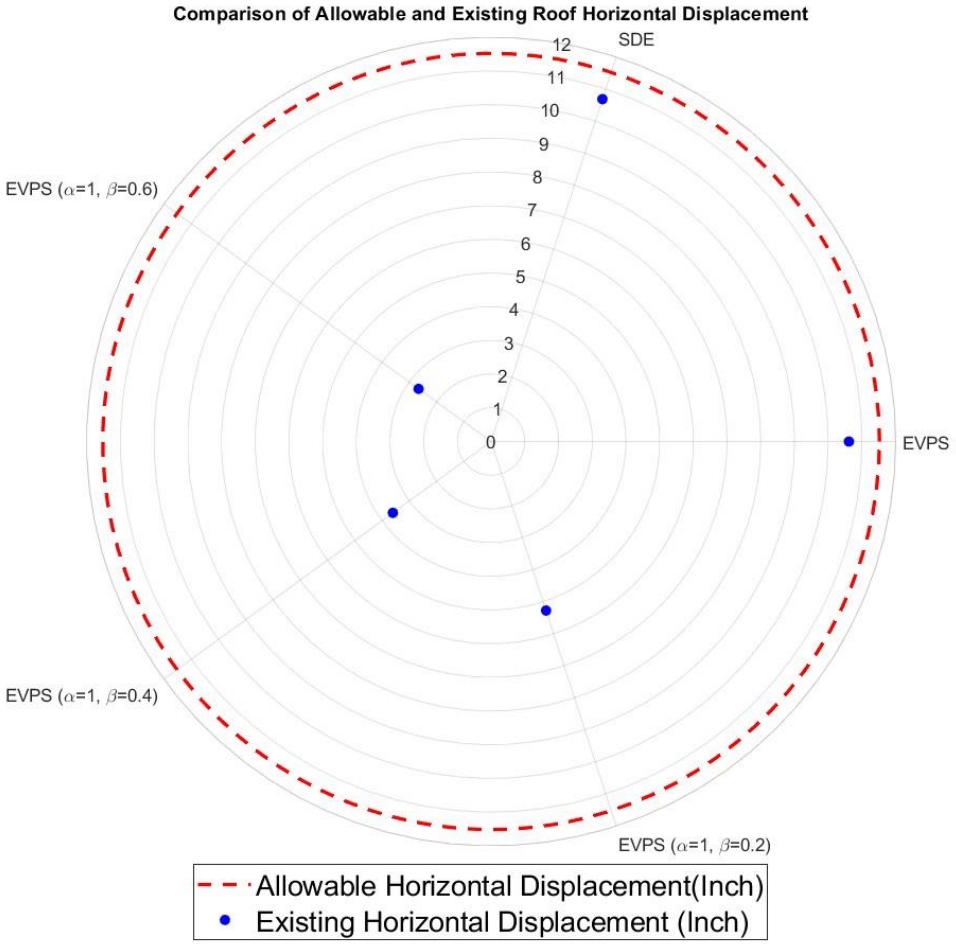

Fig. 29. Roof horizontal displacement comparison plot for different design cases of the three-bay 24-story frame.

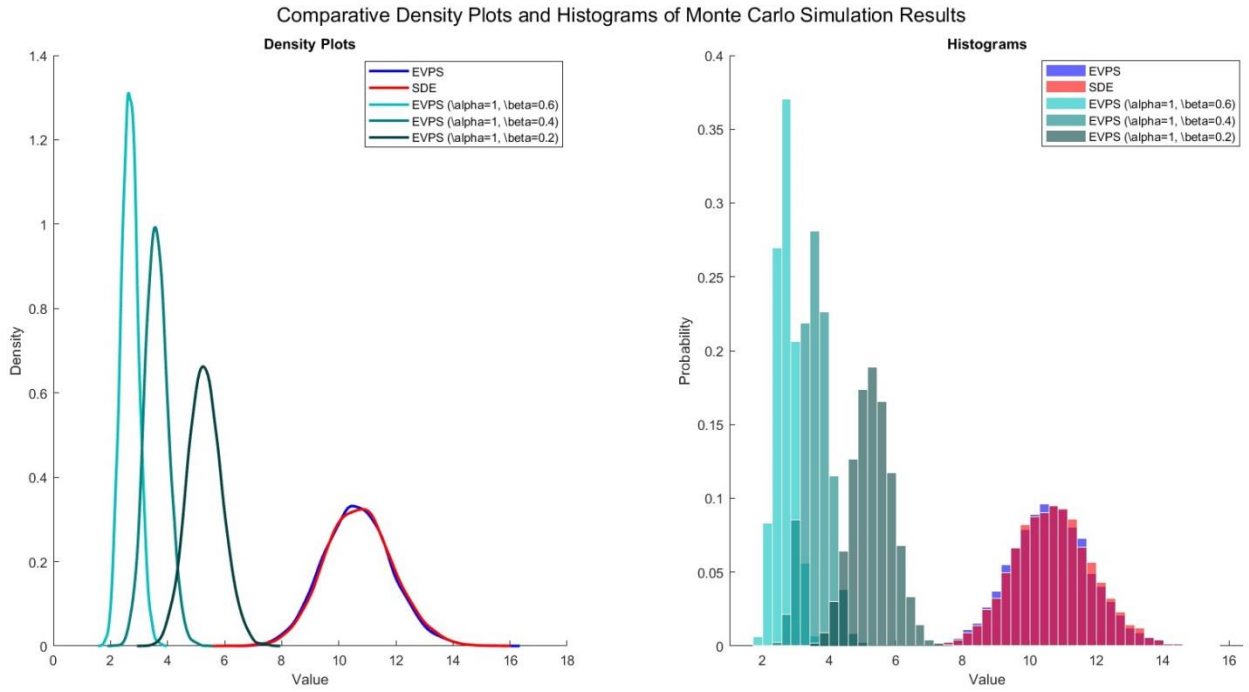

*Horizontal axis: Roof Displacement (mm); Vertical axis: Probability Density of Roof Displacement Distribution from Monte Carlo

Fig. 30. Comparative density plots and histograms of Monte Carlo simulation results for different design cases of the three-bay 24-story frame.

5.4. Discussion of results

The proposed RDO approach demonstrates consistent effectiveness across all benchmark frames. Key findings include:

1. **β coefficient effects:** Nonlinear weight increase and standard deviation reduction with diminishing returns at higher β values. Weight increases of 36-100% (β: 0→0.2), 25-29% (β:0.2→0.4), and 17-25% (β: 0.4→0.6) correspond to standard deviation reductions of 49-52%, 27-32%, and 22-27% respectively.
2. **Stress distribution:** Robust designs exhibit uniform stress distributions (0.6-0.8 range) compared to deterministic designs approaching capacity limits, providing uncertainty buffers.
3. **Displacement characteristics:** Flatter inter-story drift profiles prevent soft-story mechanisms. Narrower displacement distributions eliminate extreme values, with improvements scaling with frame height.
4. **Practical implications:** Optimal β values of 0.2-0.4 balance weight and robustness. Taller frames show greater uncertainty sensitivity. Bay configuration affects robustness efficiency, with single-bay frames requiring proportionally less weight increase for comparable robustness improvement.

6. Conclusions

This study presents comprehensive RDO strategies for steel moment-resisting frames using EVPS algorithm and MCS. Key achievements include:

- 50-60% reduction in displacement variability with 20-30% weight increase at moderate β values.
- Consistent weight-robustness relationships: 67% standard deviation reduction with 74-116%weight increase at β =0.4 across all frames.

- Practical framework allowing engineers to balance weight and robustness through β coefficient selection.
- Demonstrated scalability from 10 to 24-story structures.

Future research should extend to 3D systems, incorporate additional uncertainty sources including geometric imperfections and soil-structure interaction, and integrate dynamic/seismic analysis. The proposed RDO framework advances structural optimization and reliability-based design for steel moment-resisting frames under real-world uncertainties.

Conflicts of interest

The authors declared no potential conflicts of interest with respect to the research, authorship, and/or publication of this article.

Funding

The authors received no financial support for the research, authorship, and/or publication of this article.

Authors contribution statement

Pedram Hosseini: Conceptualization; Data curation; Formal analysis; Investigation; Methodology; Software; Validation; Roles/Writing – original draft; Supervision.

Fazeleh Sadat Lajevardi: Conceptualization; Data curation; Investigation.

Seyed Rohollah Hoseini Vaez: Conceptualization, Methodology, Supervision, Writing - Review & Editing.

References

[1] Nabati M, Gholizadeh S. PERFORMANCE-BASED OPTIMIZATION OF STEEL MOMENT FRAMES BY A MODIFIED NEWTON METAHEURISTIC ALGORITHM. Int J Optim Civ Eng 2023;13. https://doi.org/10.22068/ijoce.2023.13.2.548.

[2] Jahjouh M. An experience based artificial neural network in the design optimization of steel frames. Eng Res Express 2022;4:45031. https://doi.org/10.1088/2631-8695/aca6ce.

[3] Hasançebi O, Azad SK. An exponential big bang-big crunch algorithm for discrete design optimization of steel frames. Comput \& Struct 2012;110:167–79. https://doi.org/10.1016/j.compstruc.2012.07.014.

[4] Kaveh A, Zaerreza A. Reliability-based design optimization of the frame structures using the force method and SORA-DM framework. Structures 2022;45:814–27. https://doi.org/10.1016/j.istruc.2022.09.057.

[5] He J, Lin S, Li Y, Dong X, Chen S. Genetic Algorithm for Optimal Placement of Steel Plate Shear Walls for Steel Frames. Buildings 2022;12. https://doi.org/10.3390/buildings12060835.

[6] Hasançebi O, Carbas S. Bat inspired algorithm for discrete size optimization of steel frames. Adv Eng Softw 2014;67:173–85. https://doi.org/10.1016/j.advengsoft.2013.10.003.

[7] Le Thanh C, Sang-To T, Hoang-Le H-L, Danh T-T, Khatir S, Wahab MA. Combination of intermittent search strategy and an improve particle swarm optimization algorithm (IPSO) for damage detection of steel frame. Fract Struct Integr 2022;16:141–52. https://doi.org/10.3221/IGF-ESIS.59.11.

[8] Kaveh A, Azar BF, Hadidi A, Sorochi FR, Talatahari S. Performance-based seismic design of steel frames using ant colony optimization. J Constr Steel Res 2010;66:566–74. https://doi.org/10.1016/j.jcsr.2009.11.006.

[9] Kale BN, Aydougdu .Ibrahim, Demir E. Performance of the whale optimization algorithm in space steel frame optimization problems. Int. Conf. Harmon. Search Algorithm, 2020, p. 139–54. https://doi.org/10.1007/978-981-15-8603-3_13.

[10] Mam K, Douthe C, Le Roy R, Consigny F. Shape optimization of braced frames for tall timber buildings:

Influence of semi-rigid connections on design and optimization process. Eng Struct 2020;216:110692. https://doi.org/10.1016/j.engstruct.2020.110692.

[11] Kociecki M, Adeli H. Shape optimization of free-form steel space-frame roof structures with complex geometries using evolutionary computing. Eng Appl Artif Intell 2015;38:168–82. https://doi.org/10.1016/j.engappai.2014.10.012.

[12] Van Mellaert R, Mela K, Tiainen T, Heinisuo M, Lombaert G, Schevenels M. Mixed-integer linear programming approach for global discrete sizing optimization of frame structures. Struct Multidiscip Optim 2018;57:579–93. https://doi.org/10.1007/s00158-017-1770-9.

[13] Saldaña-Robles AL, Bustos-Gaytán A, la Peña JA, Saldaña-Robles A, Alcántar-Camarena V, Balvant in-Garcia A, et al. Structural design of an agricultural backhoe using TA, FEA, RSM and ANN. Comput Electron Agric 2020;172:105278. https://doi.org/10.1016/j.compag.2020.105278.

[14] Sadeghpour A, Ozay G. Investigating the predictive capabilities of ANN, RSM, and ANFIS in assessing the collapse potential of RC structures. Arab J Sci Eng 2024:1–22. https://doi.org/10.1007/s13369-024-09618-x.

[15] Nouri Y, Ghanbari MA, Fakharian P. An integrated optimization and ANOVA approach for reinforcing concrete beams with glass fiber polymer. Decis Anal J 2024;11:100479. https://doi.org/10.1016/j.dajour.2024.100479.

[16] Maheri MR, Safari D. Topology optimization of bracing in steel structures by genetic algorithm. Fourth Int. Conf. Adv. Steel Struct., 2005, p. 277–82. https://doi.org/10.1016/B978-008044637-0/50040-8.

[17] Ben-Tal A, Brekelmans R, Den Hertog D, Vial J-P. Globalized robust optimization for nonlinear uncertain inequalities. INFORMS J Comput 2017;29:350–66. https://doi.org/10.1287/ijoc.2016.0735.

[18] Takezawa A, Nii S, Kitamura M, Kogiso N. Topology optimization for worst load conditions based on the eigenvalue analysis of an aggregated linear system. Comput Methods Appl Mech Eng 2011;200:2268–81. https://doi.org/10.1016/j.cma.2011.03.008.

[19] Sigmund O. Manufacturing tolerant topology optimization. Acta Mech Sin 2009;25:227–39. https://doi.org/10.1007/s10409-009-0240-zDesign optimization of steel structures considering uncertainties.

[20] Papadrakakis M, Lagaros ND, Plevris V. Design optimization of steel structures considering uncertainties. Eng Struct 2005;27:1408–18. https://doi.org/10.1016/j.engstruct.2005.04.002.

[21] Wang X, Shi Y, Meng Z, Yang B, Long K. Uncertainty-oriented topology optimization of dynamic structures considering hybrid uncertainty of probability and random field. Reliab Eng \& Syst Saf 2025;256:110744. https://doi.org/10.1016/j.ress.2024.110744.

[22] Hosseini P, Kaveh A, Hoseini Vaez SR. ROBUST DESIGN OPTIMIZATION OF SPACE TRUSS STRUCTURES. Int J Optim Civ Eng 2022;12.

[23] Yadav R, Ganguli R. Reliability based and robust design optimization of truss and composite plate using particle swarm optimization. Mech Adv Mater Struct 2022;29:1892–902. https://doi.org/10.1080/15376494.2020.1843743.

[24] Dammak K, Yaich A, Hami A El, Walha L, Haddar M. An efficient optimization based on the robust hybrid method for the coupled acoustic–structural system. Mech Adv Mater Struct 2020;27:1816–26. https://doi.org/10.1080/15376494.2018.1525629.

[25] Kamel A, Dammak K, Hami A El, Jdidia M Ben, Hammami L, Haddar M. A modified hybrid method for a reliability-based design optimization applied to an offshore wind turbine. Mech Adv Mater Struct 2022;29:1229–42. https://doi.org/10.1080/15376494.2020.1811927.

[26] Yarasca J, Mantari JL, Monge JC, Hinostroza MA. A robust five-unknowns higher-order deformation theory optimized via machine learning for functionally graded plates. Mech Adv Mater Struct 2024;31:10420–35. https://doi.org/10.1080/15376494.2024.2344037.

[27] Qu X, Haftka RT. Reliability-based design optimization using probabilistic sufficiency factor. Struct Multidiscip Optim 2004;27:314–25. https://doi.org/10.1007/s00158-004-0390-3.

[28] Ito M, Kim NH, Kogiso N. Conservative reliability index for epistemic uncertainty in reliability-based design optimization. Struct Multidiscip Optim 2018;57:1919–35. https://doi.org/10.1007/s00158-018-1903-9.

[29] Yonekura K, Kanno Y. Global optimization of robust truss topology via mixed integer semidefinite programming. Optim Eng 2010;11:355–79. https://doi.org/10.1007/s11081-010-9107-1.

[30] Hosseini P, Kaveh A, Fathali MA, Vaez SRH. A two-loop RBDO approach for steel frame structures using

EVPS, GWO, and Monte Carlo simulation. Mech Adv Mater Struct 2025;32:605–24. https://doi.org/10.1080/15376494.2024.2352800.

[31] Taguchi G, Phadke MS. Quality Engineering through Design Optimization. In: Dehnad K, editor. Qual. Control. Robust Des. Taguchi Method, Boston, MA: Springer US; 1989, p. 77–96. https://doi.org/10.1007/978-1-4684-1472-1_5.

[32] Taguchi G. Introduction to quality engineering: designing quality into products and processes. 1986.

[33] Zaman K, McDonald M, Mahadevan S, Green L. Robustness-based design optimization under data uncertainty. Struct Multidiscip Optim 2011;44:183–97. https://doi.org/10.1007/s00158-011-0622-2.

[34] Parkinson A. Robust mechanical design using engineering models. J Mech Des 1995;117:48–54. https://doi.org/10.1115/1.2836470.

[35] Lagaros ND, Plevris V, Papadrakakis M. Neurocomputing strategies for solving reliability-robust design optimization problems. Eng Comput 2010;27:819–40. https://doi.org/10.1108/02644401011073674.

[36] Lagaros ND, Papadrakakis M. Robust seismic design optimization of steel structures. Struct Multidiscip Optim 2007;33:457–69. https://doi.org/10.1007/s00158-006-0047-5.

[37] Erfani T, Utyuzhnikov S V. Control of robust design in multiobjective optimization under uncertainties. Struct Multidiscip Optim 2012;45:247–56. https://doi.org/10.1007/s00158-011-0693-0.

[38] Chen W, Lewis K. Robust design approach for achieving flexibility in multidisciplinary design. AIAA J 1999;37:982–9. https://doi.org/10.2514/2.805.

[39] Chen W, Allen JK, Tsui K-L, Mistree F. A procedure for robust design: minimizing variations caused by noise factors and control factors. J Mech Des 1996;118:478–85. https://doi.org/10.1115/1.2826915.

[40] Chi H-W, Bloebaum CL. Mixed variable optimization using Taguchi's orthogonal arrays. Struct Optim 1996;12:147–52. https://doi.org/10.1007/BF01196949.

[41] Lee K-H, Eom I-S, Park G-J, Lee W-I. Robust design for unconstrained optimization problems using the Taguchi method. AIAA J 1996;34:1059–63. https://doi.org/10.2514/3.13187.

[42] Sandgren E, Cameron TM. Robust design optimization of structures through consideration of variation. Comput Struct 2002;80:1605–13. https://doi.org/10.1016/S0045-7949(02)00160-8.

[43] Doltsinis I, Kang Z. Robust design of structures using optimization methods. Comput Methods Appl Mech Eng 2004;193:2221–37. https://doi.org/10.1016/j.cma.2003.12.055.

[44] Lagaros ND, Plevris V, Papadrakakis M. Multi-objective design optimization using cascade evolutionary computations. Comput Methods Appl Mech Eng 2005;194:3496–515. https://doi.org/10.1016/j.cma.2004.12.029.

[45] Beyer H-G, Sendhoff B. Robust optimization--a comprehensive survey. Comput Methods Appl Mech Eng 2007;196:3190–218. https://doi.org/10.1016/j.cma.2007.03.003.

[46] Kang Z, Bai S. On robust design optimization of truss structures with bounded uncertainties. Struct Multidiscip Optim 2013;47:699–714. https://doi.org/10.1007/s00158-012-0868-3.

[47] Liu Z, Atamturktur S, Juang CH. Performance based robust design optimization of steel moment resisting frames. J Constr Steel Res 2013;89:165–74. https://doi.org/10.1016/j.jcsr.2013.07.011.

[48] Zhao Z, Lv G, Xu Y. Facilitate the design of residential PV using reliability-based design optimization. Renew Energy 2025;240:122144. https://doi.org/10.1016/j.renene.2024.122144.

[49] Lyu M-Z, Yang J-S, Chen J-B, Li J. High-efficient non-iterative reliability-based design optimization based on the design space virtually conditionalized reliability evaluation method. Reliab Eng \& Syst Saf 2025;254:110646. https://doi.org/10.1016/j.ress.2024.110646.

[50] Chen J, Chen Z, Jiang W, Guo H, Chen L. A reliability-based design optimization strategy using quantile surrogates by improved PC-kriging. Reliab Eng \& Syst Saf 2025;253:110491. https://doi.org/10.1016/j.ress.2024.110491.

[51] Steinacker C, Paulsen M, Schröder M, Rich J. Robust design of bicycle infrastructure networks. Sci Rep 2025;15:15471. https://doi.org/10.1038/s41598-025-99976-9.

[52] Saffari H, Zahedi MJ, Ebrahimpour N, Soleymani A. The effect of earthquake characteristics on the seismic performance of steel moment resisting frames. Int J Steel Struct 2023;23:1431–46. https://doi.org/10.1007/s13296-023-00769-5.

[53] Bakhshinezhad S, Mansouri E, Jeong S-H. Machine Learning-Aided Performance-Based Optimal Design of

Steel Moment-Resisting Frames Using NSGA-II. Nat Hazards Rev 2025;26:4025016. https://doi.org/10.1061/NHREFO.NHENG-2313.

[54] Roohbakhsh H, Vosoughi AR, Razmara Shooli A. Performance-Based Design Optimization of Corroded Special Moment--Resisting RC Frames. J Struct Des Constr Pract 2024;30:4024116. https://doi.org/10.1061/JSDCCC.SCENG-1602.

[55] Do B, Ohsaki M. Gaussian mixture model for robust design optimization of planar steel frames. Struct Multidiscip Optim 2021;63:137–60. https://doi.org/10.1007/s00158-020-02676-3.

[56] Do B, Ohsaki M, Yamakawa M. Bayesian optimization for robust design of steel frames with joint and individual probabilistic constraints. Eng Struct 2021;245:112859. https://doi.org/10.1016/j.engstruct.2021.112859.

[57] Zhang R, Hu S. Optimal design of self-centering braced frames with limited self-centering braces. J Build Eng 2024;88:109201. https://doi.org/10.1016/j.jobe.2024.109201.

[58] Soleymani A, Kontoni D-PN, Jahangir H. Random vibration-based investigation of required separation gap between adjacent buildings. Earthquakes Struct 2024;26:285–97. https://doi.org/10.12989/eas.2024.26.4.285.

[59] Soleymani A, Saffari H. A novel hybrid strong-back system to improve the seismic performance of steel braced frames. J Build Eng 2024;84:108482. https://doi.org/10.1016/j.jobe.2024.108482.

[60] Paknahd M, Hosseini P, Kaveh A, Hakim SJS. A SELF-ADAPTIVE ENHANCED VIBRATING PARTICLE SYSTEM ALGORITHM FOR STRUCTURAL OPTIMIZATION: APPLICATION TO ISCSO BENCHMARK PROBLEMS. Int J Optim Civ Eng 2025;15.

[61] Hosseini P, Kaveh A, Naghian A, Abedi A. OPTIMIZATION OF ARTIFICIAL STONE MIX DESIGN USING MICROSILICA AND ARTIFICIAL NEURAL NETWORKS. Int J Optim Civ Eng 2024;14. https://doi.org/10.22068/ijoce.2024.14.3.602.

[62] MATLAB. Version R2022a. Natick, Massachusetts, MathWorks Inc 2022.

[63] AISC. Resistance factor design specification for structural steel buildings. Am Inst Steel Constr Inc, Chicago, 2001.

[64] Kaveh A, Vaez SRH, Hosseini P. Simplified dolphin echolocation algorithm for optimum design of frame. Smart Struct Syst 2018;21:321–33. https://doi.org/10.12989/sss.2018.21.3.321.